Continence 5 (2023) 100573

Contents lists available at ScienceDirect

Continence

journal homepage: www.elsevier.com/locate/cont

Quantification of the TGF- β/SMAD fibrosis pathway in bladder wall samples from children with congenital lower urinary tract anomalies

B. Xie [a], N. Johal [b], M. Millar [c], C. Thrasivoulou [d], A.J. Kanai [e], A. Ahmed [d], C.H. Fry [a,*]

[a] School of Physiology, Pharmacology and Neuroscience, University of Bristol, UK
[b] Department of Urology, Great Ormond St Hospital, London, UK
[c] Queen's Medical Research Institute, University of Edinburgh, UK
[d] Department of Cell and Developmental Biology, UCL, UK
[e] Departments of Medicine, Pharmacology & Chemical Biology, University of Pittsburgh, Pittsburgh, USA

ARTICLE INFO

Keywords:
Bladder
Congenital anomaly
Fibrosis
TGF-β pathway
Immunofluorescence labelling

ABSTRACT

Replacement of detrusor smooth muscle (SM) with connective tissue (CT) in the bladder wall has functional consequences to lower urinary tract function, namely changes to the filling compliance and its contractile performance. In children with congenital anomalies such tissue remodelling may underlie the poor prognosis that is characteristic of a significant proportion of these patients. We have quantified the extent of CT deposition in bladder tissue samples from four age-matched (24–72 months) patient groups, namely: normally-functioning (control) bladders; bladder exstrophy, neurogenic bladders (NGB) and posterior urethral valves (PUV). In addition, using multiplex labelling we have also quantified, in neighbouring sections, expression of TGF-β, a downstream transcription factor SMAD2, connexin-43, as well as DAPI labelling of nuclear material, separately in the SM and CT regions of the detrusor layer. TGF-β receptor (TGF-βR) and Cx43 labelling were greater in SM regions of exstrophy and NGB (but not PUV) tissues when compared to control, were but unchanged in CT regions. SMAD2 labelling was similar in all groups in both SM and CT regions, with minor increases in exstrophy, NGB and PUV SM regions and small reductions in exstrophy and NGB CT regions. DAPI staining was less in CT compared with SM regions but was unchanged between patient groups. Overall, the TGF-β pathway shows variability of expression in congenital bladder anomalies, compared with control tissue, that at this period of post-natal development is greater in the extant SM layer. Antifibrotic strategies that target this pathway offer an approach to minimise fibrotic development.

1. Introduction

Several congenital anomalies are associated with bladder disorders including: the exstrophy–epispadias complex; bladder outflow obstruction from posterior urethral valves (PUV); and damage from neural tube defects such as myelomeningocoele. Despite continuing advances in surgical procedures and after-care practice [1–3] many children continue to have lower urinary tract (LUT) disorders that in a significant proportion can lead to conditions such as chronic renal failure that result in a requirement for renal replacement therapy [4]. Lower urinary tract problems can range from low-capacity bladders with decreased filling compliance to a poorly-contractile bladder but with detrusor overactivity [5–7].

Bladder wall tissue-remodelling through excessive deposition of connective tissue, or fibrosis, is a common feature of these congenital bladder anomalies [8–10]. This can be associated with greater differentiation of collagen-producing myofibroblasts; upregulation of epithelial-mesenchymal transition (EMT); and alteration of the balance between endogenous collagenases and their own inhibitors [11,12]. These imbalances could underlie the above changes to bladder function. Firstly, excessive collagen deposition will decrease bladder wall compliance (increase stiffness) as its unit elastic modulus is greater than muscle tissues that comprise most of the bladder wall [13]. However, some longer-term foetal and adult models of outflow tract obstruction show increased bladder wall compliance with sparse collagen fibrils [14,15] that suggests a decompensated stage of cellular re-modelling. Secondly, replacement of detrusor muscle with connective tissue will decrease the contractile performance of the bladder wall *per se*, as observed with detrusor preparations from paediatric exstrophy patients [16]. Thirdly, (myo)fibroblasts (interstitial cells) are linked as a functional syncitium *via* Cx43 gap junctions (detrusor myocytes are connected *via* Cx45 gap junctions [17]) and will facilitate propagation of electrical signals within the tissue mass. In overactive bladder models with greater Cx43 expression, gap junction inhibitors, such as 18β-glycyrrhetinic acid, reduce propagating spontaneous contractions [18].

* Correspondence to: School of Physiology, Pharmacology and Neuroscience, University Walk, University of Bristol, BS8 1TD, UK.
E-mail address: chris.fry@bristol.ac.uk (C.H. Fry).

https://doi.org/10.1016/j.cont.2023.100573

Characterisation of the cellular pathways that underlie fibrosis in the bladder wall will be important to develop anti-fibrotic therapies. An important question is whether the continuing development of fibrosis is more significant in the muscular or extracellular domains of bladder wall tissues and whether any changes differ in tissues from bladders with congenital anomalies. The classical fibrosis pathway [19] is mediated by transforming growth factor-β (TGF-β) cytokines that bind to a receptor (TGF-βR) and the subsequent phosphorylation of receptor-regulated SMAD proteins, such as SMAD2 [20]. The latter act as transcription factors to facilitate enhanced production of connective tissue components and other modulators that underlie fibrosis. Other pathways, such as the Wnt- and YAP/TAZ signalling, also act either co-operatively with or separately from the classical fibrosis pathway [21,22], but are beyond the scope of this current study.

The following objectives were addressed: (i) to quantify relative proportions of smooth muscle (SM) and connective tissue (CT) in samples from the bladder wall of paediatric patients with normally-functioning bladders and those with congenital anomalies (exstrophy; myelomeningocoele; PUV) affecting lower urinary tract function; (ii) to demonstrate the TGFβR/SMAD pathway in paediatric bladder wall tissues and to quantify relative levels of expression in SM and CT regions; (iii) to quantify changes to the TGFβR/SMAD pathway expression in tissues from bladders with congenital anomalies; (iv) to measure Cx43 expression and compare any changes to those in the TGFβR/SMAD pathway. We chose multiplex image analysis of protein expression in bladder wall tissue sections [23] as this allowed simultaneous evaluation of several protein targets whilst preserving the histological and topographical features of tissue sample. Thus, quantification of any regional variation of protein targets in SM and CT regions was possible.

2. Methods

Patient information, ethical approval, and preparation of tissue samples. Human tissue samples ($\lesssim$5 mm^3) were collected from the lateral wall of the bladder dome from paediatric patients undergoing procedures at Great Ormond Street Hospital (GOSH: London, UK). Prior to surgery all patients had invasive or non-invasive urodynamics prior to surgery that demonstrated reduced bladder filling compliance or increased bladder neck resistance, although quantitative data were not recorded. Three groups underwent congenital anomaly corrections; bladder exstrophy (secondary bladder reconstruction with a Kelly soft tissue procedure); neurogenic bladder (NGB) from myelomeningocoele (bladder augmentation); and bladder outflow obstruction from PUV (also bladder augmentation). A fourth, control group had normally-functioning bladders who predominantly underwent open surgery for ureteric re-implantation. All samples were collected after informed consent was obtained from patients, guardians or Gillick-competent minors before surgery. Ethical approval (04NU06) was granted by the UK Human Tissue Authority and the GOSH R&D department. Demographics of the four groups were: controls (N = 19; 13M/6F; age 37 months [26,52]); bladder exstrophy (N = 30; 17M/13F; age 66 months [29,72]); neurogenic bladder (N = 21; 6M/15F; age 59 months [36,61]); PUV (N = 15; 15M/0F; age 46 months [24,72]). All groups were age-matched; Kruskal–Wallis test, $p = 0.245$. These samples were used for various physiological and imaging experiments, but all had sub-sections taken for histological examination by immersion in 4% paraformaldehyde and then embedded in paraffin as previously described [16]. Before preparation of muscle strips (<4 mm length; ≈1.0 mm diameter) for any experimental procedure the mucosa was removed by blunt dissection: the tissue sample was always held at an unstretched length.

Tissue array (TA) construction. Subsets of tissue samples were used for image analysis. Two tissue arrays were made from paraffin-embedded tissue blocks using a manual tissue arrayer MAT1 (Beecher Instruments, USA), as described previously [24]. Demographics of patients who yielded useable cores were: controls (n = 13; 8M/5F; age 43 months [21,50]); bladder exstrophy (n = 10; 6M/4F; age 36 [27, months 72]); NGB (n = 6; 2M/4F; age 48 months [38,60]); PUV bladders (n = 8; 8M/0F; age 47 months [24,70]). There were no statistical differences in ages between the four groups (Kruskal–Wallis test; p = 0.635). Tissue array sections (8 μm) were mounted on 3-triethoxysilylpropylamine (TESPA)-coated glass slides and were used for haematoxylin & eosin (H&E) or van Gieson staining, as well as for multi-immunofluorescence labelling.

H&E and van Gieson staining; image processing. H&E staining was done for histological previews; van Gieson staining to identify predominant areas of SM or CT. For staining TA sections were deparaffinised in xylene, hydrated in ethanol from 100%–50% ethanol/water in four steps and then incubated in Weigert's iron haematoxylin solution for 15 min (Sigma-Aldrich 1.15973). Subsequently, slides were incubated in van Gieson solution (Sigma-Aldrich, HT254) for 5 min, dehydrated in ethanol, transferred to xylene and finally mounted in Eukitt® Quick-hardening mounting medium [25].

Sections were imaged at 40× magnification under bright-field conditions with a NanoZoomer Digital Pathology Scanner (Hamamatsu Photonics, Japan). Tissue core images (NDP.view2) were exported as .jpg files (11 597 × 11 597, 300 dpi) to quantify SM/CT percentages (both add to 100%) and to identify SM and CT areas for subsequent protein expression analysis. ImageJ algorithms separated red (CT) and yellow (SM) pixels to generate 8-bit grey scale images for quantification [26] – Fig. 1 (two right columns). Cores for additional protein expression quantification were part of a larger collection used for other experiments, but where SM/CT percentages were also measured: SM/CT data from the entire collection are shown.

Multiplex-immunofluorescence labelling and image processing. Three proteins were targetted with primary antibodies: TGF-βR-II (rabbit polyclonal; Abcam 61213, 1:2000); SMAD2 (rabbit polyclonal; Cell Signalling mAb3122, 1:200); and Cx43 (rabbit polyclonal; Sigma-Aldrich C6216, 1:1000): secondary antibodies were Cy5, Cy3 and FITC fluorophores, respectively. Cell nuclei were labelled with 4′,6-diamidino-2-phenylindole (DAPI) to generate a fourth fluorescence channels. Several procedures were followed to reduce potential variability of outcomes as much as possible. All slides were labelled for antibodies on a single day with a Leica BondMax™ robotic system, following prior optimisation for concentration, pH-dependence and antigen retrieval. Primary antibody stocks were made on the day of use. Labelling procedures were double-blinded; neither tissue core pathology nor antibodies were known to experimenters during data acquisition; steps in the methodology have also been described elsewhere [16,27,28].

Multiplex-immunofluorescent labelled slides were imaged using a fluorescence scanner (AxioScan Z1, Zeiss) at 20× magnification, always using the same settings. Excitation/emission wavelengths (nm) for the four channels were: 353/465 (DAPI), 493/517 (Cx43), 553/568 (SMAD2) and 653/668 (TGF-β). Fluorescence channels were optimised for excitation/emission ranges as well as intensities to reduce overlap between channels and bleed-through from each channel. Protein images were opened in Zeiss ZEN 3.1 software (blue edition) for subsequent analysis. Corrections were made for images with no primary antibodies and autofluorescence background. For each core, ten circular regions of interest (RoIs, 60 μm diameter) were randomly chosen; five each in SM and CT areas, as determined above. Fluorescence intensities for each channel were measured by counting the number of pixels in each RoI with the open-source Fiji-ImageJ program. Steps in the methodology have also been detailed elsewhere [16,27,28].

Data presentation and analysis. Data sets are expressed as median values [25,75%] interquartile ranges, as not all data sets were normally-distributed using Shapiro–Wilks tests. Differences between sets were tested by non-parametric ANOVA and *post-hoc* Mann–Whitney U-tests (www.medcalc.org); null hypotheses were rejected at $p < 0.05$. The variability of values in data sets (*var.*) were calculated as

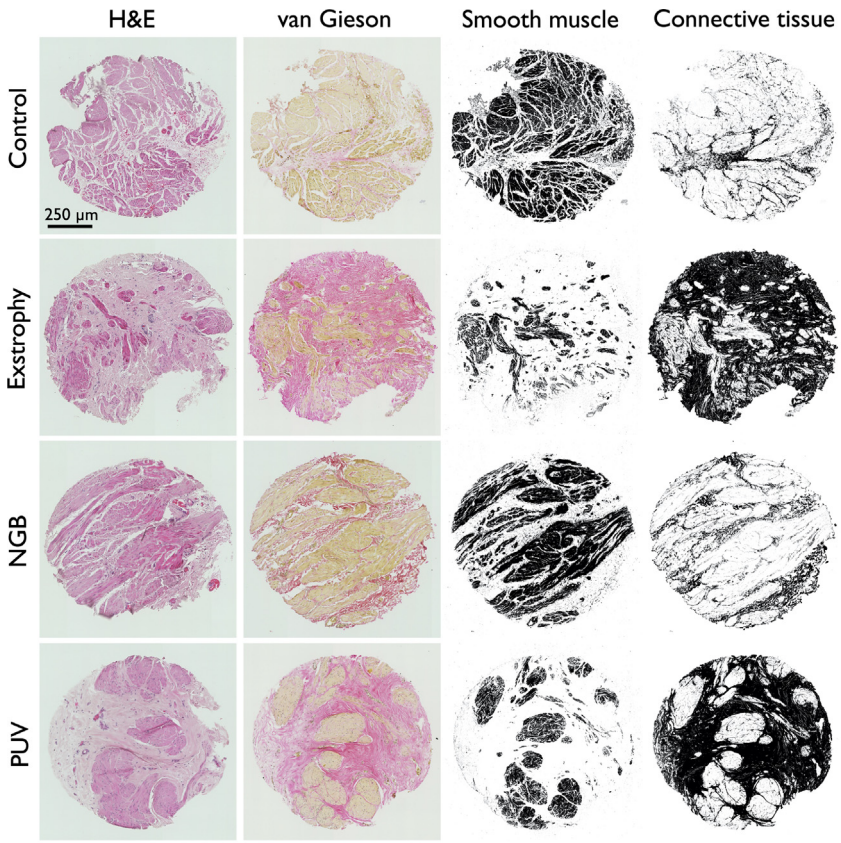

Fig. 1. H&E and van Gieson stained images of sections from the same tissue sample (two left columns) from control, exstrophy, NGB, and PUV tissue samples. The two right-hand columns are 8-bit grey scale images of the smooth muscle and connective tissue components of the van Gieson stained images and used to measure the percentages of smooth muscle and connective tissue in the tissue samples. (For interpretation of the references to colour in this figure legend, the reader is referred to the web version of this article.)

MADM/median values, where MADM (median absolute deviation from the median) was calculated as:

$$\text{MADM} = \text{median}(|x_i - \text{median}(x)|),$$

for all x_i in a data set; |..| is the modulus of a number. The value of *var.* is parallelled by a coefficient of variation (SD/mean) of a normally-distributed data set; values <0.25 were taken as low variability.

3. Results

Measurement of smooth muscle and connective tissue content. Fig. 1 shows representative near-consecutive sections stained with H&E (far left) or van Gieson (second left) from the four groups. The two right-hand columns show 8-bit grey-scale images of the smooth muscle (SM, yellow) or connective tissue (CT, red) regions of the van Gieson-stained sections to calculate the respective contributions of the two regions.

Fig. 2 shows the percentage SM content of tissue cores, the remainder classified as CT, from the four bladder conditions investigated here. Tissue from control bladders had significantly more smooth muscle (66.1% [60.7,76.8], $n = 19$, *var.* = 0.159) compared to that from bladder exstrophy (34.9% [26.2,42.7], $n = 30$; $p < 0.0001$, *var.* = 0.240), NGB (50.7% [41.1,54.3], $n = 21$; $p < 0.01$, *var.* = 0.210), or PUV bladders (49.8% [45.8,57.4], $n = 15$, *var.* = 0.143; $p < 0.001$). Moreover, SM content was significantly less in bladder exstrophy samples compared to those from neuropathic ($p < 0.005$) or PUV bladders ($p < 0.05$). The variability of these data (*var.* – see Methods and Supplementary Table 1) was greatest in exstrophy samples compared to controls and reflects a decreased homogeneity of exstrophy samples; intermediate *var.* values were recorded in samples from neuropathic, but not PUV bladder, samples.

Regional differences of TGFβR, SMAD3 and Cx43 protein labelling in bladder tissue cores. Fig. 3 shows low-power images of multiplex-labelled

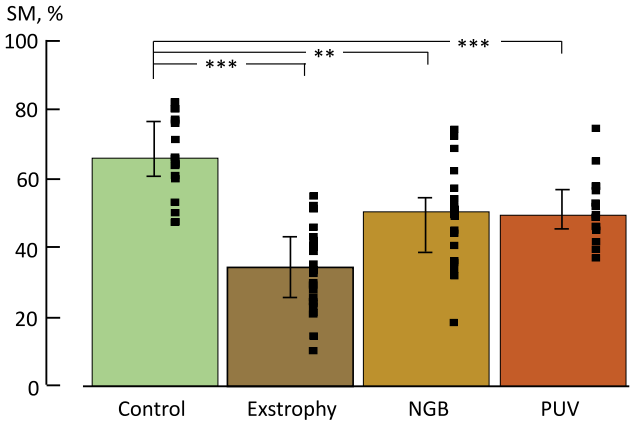

Fig. 2. Percentage smooth muscle content of tissue cores from control, exstrophy, neurogenic (NGB) and posterior urethral valves (PUV) bladders. Median data [25,75% interquartiles]. $^{**}p < 0.01$; $^{***}p < 0.001$ *vs.* control.

core sections from exstrophy, NGB and PUV samples (top row) and in the centre an image from a control sample. Separate images of the control core in each of the four colour channels for the three proteins (TGFβR, purple: SMAD2, orange; and Cx43, green) as well as DAPI (blue) are seen around the multicolour central image. Overall SM appears green due to a preponderant Cx43 signal and CT a more mixed purple colour due to TGFβR and SMAD2 signals especially evident in the non-muscle areas. DAPI staining is homogeneous throughout the SM and CT regions of the section. Shown also in the bottom row are high-power images of a SM region (left) and a CT region (right). These

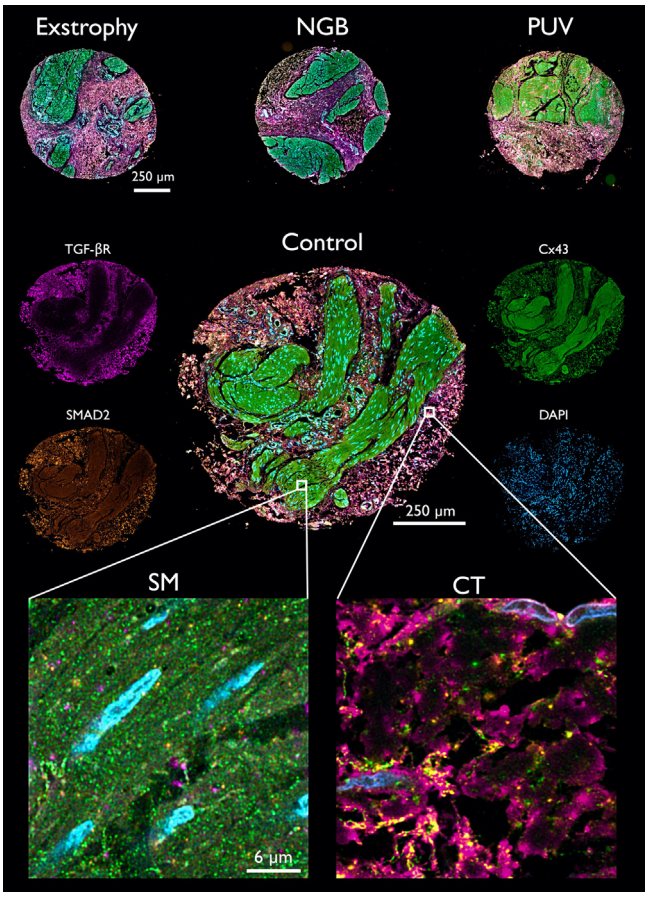

Fig. 3. Multilabelled images of different bladder core sections from the four patient groups. The top row shows low power sections from exstrophy, NGB and PUV bladders. A control sample image is shown below surrounded by individual colour channels for that same section: purple/pink, TGFβR; orange/yellow, SMAD2; green, Cx43; blue, DAPI. In the multilabelled images, the muscle area is a green colour from the preponderant intensity of the Cx43 label; the pink/purple areas correspond to connective tissue. High-power images at the bottom are 30 × 30 μm fields of a smooth muscle (SM, left) and a connective tissue (CT, right) region of the control tissue section. These lie within 60 μm diameter regions of interest used for semi-quantitative analysis. (For interpretation of the references to colour in this figure legend, the reader is referred to the web version of this article.)

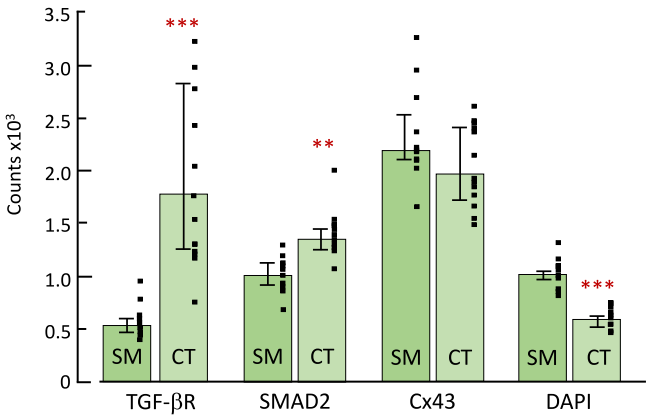

Fig. 4. Counts of three protein labels (TGFβR, SMAD2 and Cx43) and DAPI staining in cores from control bladders. Data points represent averaged counts in five regions of interest each in smooth muscle (SM) and connective tissue (CT) regions from 11 separate tissue cores. Median data [25,75% interquartiles]. $^{**}p < 0.01$; $^{***}p < 0.001$ CT *vs.* SM.

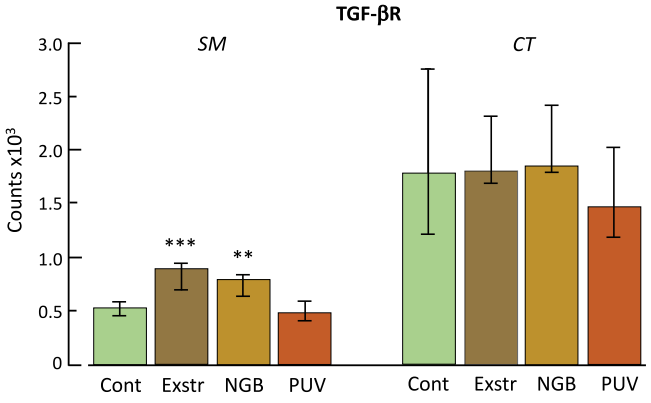

Fig. 5. Counts of TGFβR label from Control (con), Exstrophy (Exstr), Neurogenic (NGB) and Posterior urethral valve (PUV) bladders. Left-hand panel; smooth muscle data: right-hand panel; connective tissue data. Median data [25,75% interquartiles]. $^{**}p < 0.01$; $^{***}p < 0.001$ *vs.* Control. (For interpretation of the references to colour in this figure legend, the reader is referred to the web version of this article.)

images are 30 × 30 μm fields within 60 μm diameter regions of interest used for analysis.

Regional differences of TGFβR, SMAD2 and Cx43 protein labelling in control bladder tissue cores. Protein labelling of TGFβR, SMAD2 and Cx43, as well as the nuclear DAPI label, was measured in five ROIs in both SM and CT regions of each core. Median values for the two regions were compared in tissue cores from control bladders. TGFβR and SMAD2 expression was significantly greater in CT compared to SM regions, despite significantly less DAPI labelling (Fig. 4). However, there was no difference in Cx43 labelling between the two regions. Data variability (*var.*) ranged between 0.042 – 0.171 in all data sets, except with TGFβR counts from CT regions where it was significantly greater (*var.* = 0.429; $p < 0.05$ – for values see Supplementary Table 1).

TGF-βR labelling in bladder samples. Fig. 5 shows quantification of TGFβR labelling in the four patient groups for the SM regions (left) and the CT regions (right). In all groups labelling was greater in the CT regions. In SM regions TGFβR labelling was greater in exstrophy ($p < 0.001$) and NGB ($p < 0.01$) samples compared to control tissue. However, there was no comparable increase in PUV samples. By contrast, TGFβR labelling in connective tissue regions was not significantly different in any of the four patient groups. Connective tissue TGFβR labelling in control tissue was more variable than in any other group (*var.* = 0.429, but was also larger for exstrophy and PUV data than most other data sets) - see Supplementary Table 1 - and would have masked small variations between data from different patient groups. DAPI labelling was similar between patient groups from SM and from CT regions and is not further reported.

SMAD2 labelling in bladder samples. By contrast, the magnitude of SMAD2 labelling was more similar between SM and CT regions in all patient groups, although significantly greater in connective tissue regions from control tissue ($p < 0.01$; Fig. 4). Comparison of data from the four patient groups showed (Fig. 6), in SM regions, small but significantly ($p < 0.05$), greater values in exstrophy, NGB and PUV samples compared to control. In CT regions there was slightly, but significantly, less ($p < 0.05$), labelling in exstrophy and NGB samples, but not PUV samples, compared to control: *var.* values were generally small, except for PUV samples.

Cx43 labelling in bladder samples. In smooth muscle regions Cx43 labelling was significantly greater with tissue from exstrophy and NGB bladders ($p < 0.001$), as well as PUV tissue ($p < 0.01$) – Fig. 7. There were however, no significant differences between the four patient groups in the connective tissue regions: *var.* values were generally small.

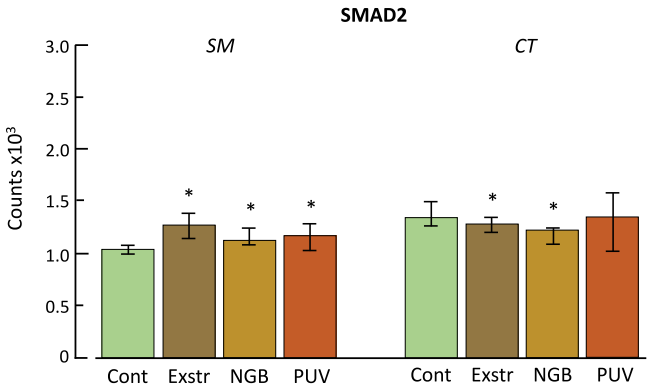

Fig. 6. Counts of SMAD2 label from Control (con), Exstrophy (Exstr), Neurogenic (NGB) and Posterior urethral valve (PUV) bladders. Left-hand panel; smooth muscle data: right-hand panel; connective tissue data. Median data [25,75% interquartiles]. *$p < 0.05$ *vs.* Control. (For interpretation of the references to colour in this figure legend, the reader is referred to the web version of this article.)

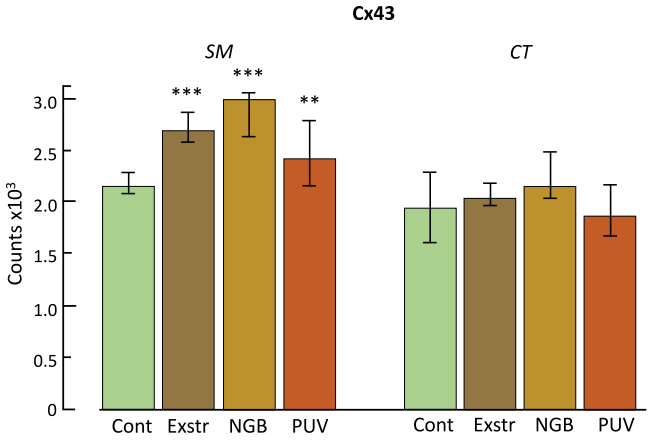

Fig. 7. Counts of Cx43 label from Control (con), Exstrophy (Exstr), Neurogenic (NGB) and Posterior urethral valve (PUV) bladders. Left-hand panel; smooth muscle data: right-hand panel; connective tissue data. Median data [25,75% interquartiles]. **$p < 0.01$; ***$p < 0.001$ *vs.* Control. (For interpretation of the references to colour in this figure legend, the reader is referred to the web version of this article.)

4. Discussion

Bladder wall tissue from the detrusor layer has a decreased proportion of muscle tissue in all three congenital anomalies studied compared with that from normally-functioning (control) bladders. Moreover, SM loss was greatest in exstrophy bladder samples. Although SM proportion increases with age in paediatric patients [24], this was not a confounding factor here, as all four groups were age-matched. There was, however, a larger variability of values in the exstrophy and neuropathic bladder groups as evidenced by the larger *var.* scores, especially in exstrophy tissues and suggests that raised CT deposition is variable between different bladders.

The particular protein targets were chosen to represent initial components of a canonical fibrosis pathway (the TGFβR and SMAD2), and which is abundant in interstitial cells (Cx43). Data from all four groups showed that TGFβ and SMAD2 were expressed more in the CT fraction compared with the SM domain, despite reduced DAPI staining. Cx43 was labelled to a similar extent in both fractions and suggests substantial infiltration of detrusor bundles with say interstitial cells or other cells transitioning from fibroblasts and to myofibroblasts [29]: note the major gap junction connexin between detrusor myocytes is Cx45 [30]. Measurement of this differential distribution of TGFβ and SMAD2 in CT and SM regions was possible by the multiplex labelling imaging method used here and offers an advantage over other quantitative protein assay methods, such as Western blotting that cannot distinguish so readily between changes to protein expression in discrete areas of a complex tissue. Other models of bladder fibrosis have also described increased TGFβR expression [31,32], but this may be due merely to the greater proportion of CT and not a unit upregulation of TGFβR as recorded here.

With tissue from congenital anomaly bladders, in comparison with control tissue, there were dissimilar changes to protein labels in CT and SM layers. With tissue from exstrophy and neurogenic bladders, in comparison with control, expression of TGFβR and SMAD2 was enhanced in SM regions but was less in CT regions. A similar pattern was observed with Cx43 in exstrophy tissue, but with neurogenic bladder tissue an increase only in SM regions was observed: the extent of DAPI staining was unchanged in these pathologies. A somewhat different pattern emerged in PUV bladder tissue: smaller proportional changes of SMAD2 and Cx43 in SM regions, but with no changes in CT regions. Such a disparity with different anomalies has been observed with other labels. For example, matrix metalloproteinase-7 (MMP7) whose main function is to break down extracellular matrix, is overall increased in several adult fibrotic conditions [33,34] but is reduced in tissue from exstrophy bladders (16), unchanged in NGB [10] and increased in PUV bladders (9). Similarly, cyclin D1 which allows cells to progress through the cell cycle [35], is unchanged in tissue from exstrophy and NGB, but is reduced in PUV bladders [9,10,16]. This raises the possibility that the rate of connective tissue deposition is variable within different regions of a complex tissue such as the bladder wall. Furthermore, changes may occur over variable time-frames during post-natal tissue re-modelling from different congenital anomalies, but in this study we age-matched patient age between the different groups donating tissue.

Activation of the TGF-β/SMAD pathway is the best characterised mechanism for fibrotic development and is known to be active in the paediatric bladder. Attenuation of this pathway is a direct approach to limit the development of fibrosis in bladder dysfunction in the pathologies described above. Different therapeutic possibilities have been described, although with limited evidence of effectiveness [36]. In addition, selective reversal in specific tissues always remains a problem. An alternative approach may be to evaluate the function of associated pathways that either regulate fibrosis directly or interact with the TGF-β/SMAD pathway. For example, activation of the Wnt/β-catenin-signalling acts as a regulator of fibrosis [21,37] through attenuation of cytosolic β-catenin degradation. Moreover, there is a positive interaction between TGF-β/SMAD and Wnt ligands/β-catenin pathways to augment fibrosis [21,38]. Bladder fibrosis, induced by X-ray irradiation, can also be ameliorated in adult mice by relaxin, a small polypeptide member of the insulin superfamily. Moreover, this was associated, by restoration of bladder compliance and reduction of overactive bladder contractions [39]. SMAD2 phosphorylation is also attenuated by activation of the nNOS/NO-soluble guanylate cyclase-cGMP system by the relaxin receptor [40,41]. Several other potential antifibrotic pathways have also been described [42].

Changes to the activities of fibrosis pathways is one route for raised connective tissue deposition, but an alternative is a decrease of the activity of intrinsic collagenases, such as MMP7. However, variable changes to MMP7 labelling in different anomalies compared with control, as described above, do not support a hypothesis that variation of its expression is a major determinant of excessive fibrosis in these conditions.

Overall, bladder wall fibrosis is a feature of several different congenital bladder anomalies and associated with increased passive stiffness [9,10,16]. The canonical TGF-β/SMAD pathway is expressed throughout the detrusor layer, but to a greater extent in the CT component. However, in the time-frame associated with these studies (40–60 days *post partum*) there was down-regulation in CT but upregulation in detrusor muscle in samples from exstrophy and NGB, compared with normally-functioning bladders. However, in PUV-obstructed bladders

such up- and down-regulation was less evident. Cx43 was abundantly and evenly distributed throughout the detrusor layer and may not be useful as a differential marker of fibrosis.

Limitations. Confounding variables that may limit data interpretation arise from the patient cohorts, tissue and the semiquantitative data that are provided. Patients in the four groups were age-matched, but not gender-matched; for example PUV occurs only in males. Sample sizes were too small to allow sub-division of data from different sexes. It was not possible to orientate the tissue samples in the same way dimension relative to their original position in the bladder wall in construction of the tissue array, due to the small size of the original samples. However, care was taken not to unduly stretch the samples during dissection into samples. Finally, it is appreciated that multiplex immunofluorescence is a semi-quantitative technique and differences in signal intensity between different proteins do not reflect their relative abundance or its activity.

Conclusions. Several questions remain in the context of development of antifibrosis strategies: is excessive connective tissue deposition complete at this time, still developing or resolving in some congenital anomalies; what are the roles of additional pathways in regulating the TGF-β/SMAD pathway; are there male–female differences (all PUV samples were from males, the other groups were of mixed sex); and are there significant associations between urodynamic indices of bladder function and the extent of connective tissue deposition?

Declaration of competing interest

The authors declare that they have no known competing financial interests or personal relationships that could have appeared to influence the work reported in this paper.

Acknowledgments

We are grateful for funding from The Urological Foundation, The Royal College of Surgeons of England and the National Institutes of Health, USA (R01 DK098361).

Appendix A. Supplementary data

Supplementary material related to this article can be found online at https://doi.org/10.1016/j.cont.2023.100573.

References

[1] J.H. Kelly, K. Taghavi, I. Mushtaq, Justin H Kelly and his procedure for bladder exstrophy and epispadias, J. Pediatr. Surg. 57 (2022) 314–321, http://dx.doi.org/10.1016/j.jpedsurg.2021.09.005.

[2] K. Taghavi, L.A. O'Hagan, J. Bortagaray, A. Bouty, J.M. Hutson, M. O'Brien, Complication profile of augmentation cystoplasty in contemporary paediatric urology: a 20-year review, ANZ J. Surg. 91 (2021) 1005–1010, http://dx.doi.org/10.1111/ans.16736.

[3] V. Chalfant, C. Riveros, A. Elshafei, A.A. Stec, An evaluation of perioperative surgical procedures and complications in classic bladder exstrophy patients Using the National Surgical Quality Improvement Program-Pediatric (NSQIP-P), J. Pediatr. Urol. 18 (2022) 354.e1–354.e7, http://dx.doi.org/10.1016/j.jpurol.2022.03.006.

[4] D.J. McLeod, K.M. Szymanski, E. Gong, C. Granberg, P. Reddy, Y. Sebastião, M. Fuchs, P. Gargollo, B. Whittam, BA. van der Brink, Pediatric Urology Midwest Alliance (PUMA). Renal replacement therapy and intermittent catheterization risk in posterior urethral valves, Pediatrics 143 (2019) e20182656, http://dx.doi.org/10.1542/peds.2018-2656.

[5] N. Handa, D.K. Bowen, J. Guo, D.I. Chu, S.J. Kielb, Long-term kidney outcomes in exstrophy-epispadias complex: how patients present as adults, Urology 154 (2021) 333–337, http://dx.doi.org/10.1016/j.urology.2021.01.033.

[6] J.G. Borer, R. Strakosha, S.B. Bauer, D.A. Diamond, M. Pennison, I. Rosoklija, S. Khoshbin, Combined cystometrography and electromyography of the external urethral sphincter following complete primary repair of bladder exstrophy, J. Urol. 191 (5 Suppl) (2014) 1547–1552, http://dx.doi.org/10.1016/j.juro.2013.10.104.

[7] A. Korzeniecka-Kozerska, T. Porowski, J. Bagińska, A. Wasilewska, Urodynamic findings and renal function in children with neurogenic bladder after myelomeningocele, Urol. Int. 95 (2015) 146–152, http://dx.doi.org/10.1159/000431184.

[8] B.R. Lee, E.J. Perlman, A.W. Partin, R.D. Jeffs, J.P. Gearhart, Evaluation of smooth muscle and collagen subtypes in normal newborns and those with bladder exstrophy, J. Urol. 156 (1996) 2034–2036.

[9] N. Johal, K. Cao, C. Arthurs, M. Millar, C. Thrasivoulou, A. Ahmed, R.I. Jabr, D. Wood, P. Cuckow, C.H. Fry, Contractile function of detrusor smooth muscle from children with posterior urethral valves - the role of fibrosis, J. Pediatr. Urol. 17 (2021) 100.e1–100.e10, http://dx.doi.org/10.1016/j.jpurol.2020.11.001.

[10] N. Johal, K.X. Cao, B. Xie, M. Millar, R. Davda, A. Ahmed, A.J. Kanai, D.N. Wood, R.I. Jabr, C.H. Fry, Contractile and structural properties of detrusor from children with neurogenic lower urinary tract dysfunction, Biol. (Basel) 10 (2021) 863, http://dx.doi.org/10.3390/biology10090863.

[11] X.W. Jin, Q.Z. Wang, Y. Zhao, B.K. Liu, X. Zhang, X.J. Wang, G.L. Lu, J.W. Pan, Y. Shao, An experimental model of the epithelial to mesenchymal transition and pro-fibrogenesis in urothelial cells related to bladder pain syndrome/interstitial cystitis, Transl. Androl. Urol. 10 (2021) 4120–4131, http://dx.doi.org/10.21037/tau-21-392.

[12] B. Peyronnet, C. Richard, C. Bendavid, F. Naudet, J. Hascoet, C. Brochard, N. Senal, M. Jezequel, Q. Alimi, Z.E. Khene, A. Corlu, B. Clément, L. Siproudhis, G. Bouguen, J. Kerdraon, A. Manunta, X. Gamé, Urinary TIMP-2 and MMP-2 are significantly associated with poor bladder compliance in adult patients with spina bifida, Neurourol. Urodyn. 38 (2019) 2151–2158, http://dx.doi.org/10.1002/nau.24163.

[13] R. Akhtar, M.J. Sherratt, J.K. Cruickshank, B. Derby, Characterizing the elastic properties of tissues, Mater. Today 14 (2011) 96–105, http://dx.doi.org/10.1016/S1369-7021(11)70059-1.

[14] N. Thiruchelvam, C. Wu, A. David, A.S. Woolf, P.M. Cuckow, C.H. Fry, Neurotransmission and viscoelasticity in the ovine fetal bladder after in utero bladder outflow obstruction, Am. J. Physiol. Regul. Integr. Comp. Physiol. 284 (2003) R1296–R1305, http://dx.doi.org/10.1152/ajpregu.00688.2002.

[15] L. Johnston, R.M. Cunningham, J.S. Young, C.H. Fry, G. McMurray, R. Eccles, K.D. McCloskey, Altered distribution of interstitial cells and innervation in the rat urinary bladder following spinal cord injury, J. Cell. Mol. Med. 16 (2012) 1533–1543, http://dx.doi.org/10.1111/j.1582-4934.2011.01410.x.

[16] N.S. Johal, C. Arthurs, P. Cuckow, K. Cao, D.N. Wood, A. Ahmed, Fry C.H., Functional histological and molecular characteristics of human exstrophy detrusor, J. Pediatr. Urol. 15 (2019) 154.e1–154.e9, http://dx.doi.org/10.1016/j.jpurol.2018.12.004.

[17] G.P. Sui, S.R. Coppen, E. Dupont, S. Rothery, J. Gillespie, D. Newgreen, N.J. Severs, C.H. Fry, Impedance measurements and connexin expression in human detrusor muscle from stable and unstable bladders, BJU Int. 92 (2003) 297–305, http://dx.doi.org/10.1046/j.1464-410x.2003.04342.x.

[18] Y. Ikeda, C.H. Fry, F. Hayashi, D. Stolz, D. Griffiths, A. Kanai, Role of gap junctions in spontaneous activity of the rat bladder, Am. J. Physiol. Renal. Physiol. 293 (2007) F1018–F1025, http://dx.doi.org/10.1152/ajprenal.00183.2007.

[19] J. Massagué, TGFβ signalling in context, Nat. Rev. Mol. Cell Biol. 13 (2012) 616–630, http://dx.doi.org/10.1038/nrm3434.

[20] P.M. Tang, Y.Y. Zhang, T.S. Mak, P.C. Tang, X.R. Huang, H.Y. Lan, Transforming growth factor-β signalling in renal fibrosis: from Smads to non-coding RNAs, J. Physiol. 596 (2018) 3493–3503, http://dx.doi.org/10.1113/JP274492.

[21] A. Akhmetshina, K. Palumbo, C. Dees, C. Bergmann, P. Venalis, P. Zerr, A. Horn, T. Kireva, C. Beyer, J. Zwerina, H. Schneider, A. Sadowski, M.O. Riener, O.A. MacDougald, O. Distler, G. Schett, J.H. Distler, Activation of canonical Wnt signalling is required for TGF-β-mediated fibrosis, Nature Commun. 3 (2012) 735, http://dx.doi.org/10.1038/ncomms1734.

[22] X. He, M.F. Tolosa, T. Zhang, S.K. Goru, L.Ulloa. Severino, P.S. Misra, C.M. McEvoy, L. Caldwell, S.G. Szeto, F. Gao, X. Chen, C. Atin, V. Ki, N. Vukosa, C. Hu, J. Zhang, C. Yip, A. Krizova, J.L. Wrana, D.A. Yuen, Myofibroblast YAP/TAZ activation is a key step in organ fibrogenesis, JCI Insight 7 (2022) e146243, http://dx.doi.org/10.1172/jci.insight.146243.

[23] C. Arthurs, B.N. Murtaza, C. Thomson, K. Dickens, R. Henrique, H.R.H. Patel, M. Beltran, M. Millar, C. Thrasivoulou, A. Ahmed, Expression of ribosomal proteins in normal and cancerous human prostate tissue, PLoS One 12 (2017) e0186047, http://dx.doi.org/10.1371/journal.pone.0186047.

[24] N. Johal, D.N. Wood, A.S. Wagg, P. Cuckow, C.H. Fry, Functional properties and connective tissue content of pediatric human detrusor muscle, Am. J. Physiol. Renal. Physiol. 307 (2014) F1072–F1079, http://dx.doi.org/10.1152/ajprenal.00380.2014.

[25] S.A. Benard, O.O. Afolabi, A.A. Fowotade, J.O. Okoye, O.A. Olutunde, J.K. Bankole, Hibiscus-van Gieson stain for collagen fibres, Afr. J. Cell. Pathol. 9 (2017) 1–4, http://dx.doi.org/10.5897/ajcpath.

[26] C. Arthurs, A. Suarez-Bonnet, C. Willis, B. Xie, N. Machulla, T.S. Mair, K. Cao, M. Millar, C. Thrasivoulou, S.L. Priestnall, A. Ahmed, Equine penile squamous cell carcinoma: expression of biomarker proteins and EcPV2, Sci. Rep. 10 (2020) 7863, http://dx.doi.org/10.1038/s41598-020-64014-3.

[27] A.J. Symes, M. Eilertsen, M. Millar, J. Nariculam, A. Freeman, M. Notara, M.R. Feneley, H.R. Patel, J.R. Masters, A. Ahmed, Quantitative analysis of BTF3, HINT1, NDRG1 and ODC1 protein over-expression in human prostate cancer tissue, PLoS One 8 (12) (2013) e84295, http://dx.doi.org/10.1371/journal.pone.0084295.

[28] M. Arya, C. Thrasivoulou, R. Henrique, M. Millar, R. Hamblin, R. Davda, K. Aare, J.R. Masters, C. Thomson, A. Muneer, H.R. Patel, A. Ahmed, Targets of Wnt/z-catenin transcription in penile carcinoma, PLoS One 10 (4) (2015) e0124395, http://dx.doi.org/10.1371/journal.pone.0124395.

[29] L. Cao, Y. Chen, L. Lu, Y. Liu, Y. Wang, J. Fan, Y. Yin, Angiotensin II upregulates fibroblast-myofibroblast transition through Cx43-dependent CaMKII and TGF-β1 signaling in neonatal rat cardiac fibroblasts, Acta. Biochim. Biophys. Sin. 50 (2018) 843–852, http://dx.doi.org/10.1093/abbs/gmy090.

[30] G.P. Sui, S.R. Coppen, E. Dupont, S. Rothery, J. Gillespie, D. Newgreen, N.J. Severs, C.H. Fry, Impedance measurements and connexin expression in human detrusor muscle from stable and unstable bladders, BJU Int. 92 (2003) 297–305, http://dx.doi.org/10.1046/j.1464-410x.2003.04342.x.

[31] J.F. Jhang, H.J. Wang, Y.H. Hsu, L.A. Birder, H.C. Kuo, Upregulation of neurotrophins and transforming growth factor-β expression in the bladder may lead to nerve hyperplasia and fibrosis in patients with severe ketamine-associated cystitis, Neurourol. Urodyn. 38 (2019) 2303–2310, http://dx.doi.org/10.1002/nau.24139.

[32] Y. Chen, Y. Ma, Y. He, D. Xing, E. Liu, X. Yang, W. Zhu, Q. Wang, J.G. Wen, The TGF-β1 pathway is early involved in neurogenic bladder fibrosis of juvenile rats, Pediatr. Res. 90 (2021) 759–767, http://dx.doi.org/10.1038/s41390-020-01329-x.

[33] C.C. Huang, J.H. Chuang, M.H. Chou, C.L. Wu, C.M. Chen, C.C. Wang, Y.S. Chen, C.L. Chen, M.H. Tai, Matrilysin (MMP-7) is a major matrix metalloproteinase upregulated in biliary atresia-associated liver fibrosis, Mod. Pathol. 18 (2005) 941–950, http://dx.doi.org/10.1038/modpathol.3800374.

[34] B. Ke, C. Fan, L. Yang, X. Fang, Matrix metalloproteinases-7 and kidney fibrosis, Front. Physiol. 8 (2017) 21, http://dx.doi.org/10.3389/fphys.2017.00021.

[35] M. Fu, C. Wang, Z. Li, T. Sakamaki, R.G. Pestell, Cyclin D1: normal and abnormal functions, Endocrinology 145 (2004) 5439–5447, http://dx.doi.org/10.1210/en.2004-0959.

[36] Y.T. Lu, S.J. Tingskov, J.C. Djurhuus, R. Nørregaard, L.H. Olsen, Can bladder fibrosis in congenital urinary tract obstruction be reversed? J. Pediatr. Urol. 13 (2017) 574–580, http://dx.doi.org/10.1016/j.jpurol.2017.08.013.

[37] D. Choi, J.Y. Han, J.H. Shin, C.M. Ryu, H.Y. Yu, A. Kim, S. Lee, J. Lim, D.M. Shin, M.S. Choo, Down-regulation of WNT11 is associated with bladder tissue fibrosis in patients with interstitial cystitis/bladder pain syndrome without Hunner lesion, Sci. Rep. 8 (2018) 9782, http://dx.doi.org/10.1038/s41598-018-28093-7.

[38] M. Padwal, L. Liu, P.J. Margetts, The role of WNT5a and Ror2 in peritoneal membrane injury, J. Cell. Mol. Med. 24 (2020) 3481–3491, http://dx.doi.org/10.1111/jcmm.15034.

[39] Y. Ikeda, I.V. Zabbarova, L.A. Birder, P. Wipf, S.E. Getchell, P. Tyagi, C.H. Fry, M.J. Drake, A.J. Kanai, Relaxin-2 therapy reverses radiation-induced fibrosis and restores bladder function in mice, Neurourol. Urodyn. 37 (2018) 2441–2451, http://dx.doi.org/10.1002/nau.23721.

[40] C.S. Samuel, S.G. Royce, T.D. Hewitson, K.M. Denton, T.E. Cooney, R.G. Bennett, Anti-fibrotic actions of relaxin, Br. J. Pharmacol. 174 (2017) 962–976, http://dx.doi.org/10.1111/bph.13529.

[41] B.S. Chow, E.G. Chew, C. Zhao, R.A. Bathgate, T.D. Hewitson, C.S. Samuel, Relaxin signals through a RXFP1-pERK-nNOS-NO-cGMP-dependent pathway to up-regulate matrix metallo-proteinases, PLoS One 7 (2012) 42714, http://dx.doi.org/10.1371/journal.pone.0042714.

[42] C.H. Fry, B. Chakrabarty, H. Hashitani, K.E. Andersson, K. McCloskey, R.I. Jabr, M.J. Drake, New targets for overactive bladder-ICI-RS 2109, Neurourol. Urodyn. 39 Suppl 3 (2020) S113–S121, http://dx.doi.org/10.1002/nau.24228.